RESEARCH ARTICLE | MARCH 28 2023

Stochastic transitions: Paths over higher energy barriers can dominate in the early stages

S. P. Fitzgerald ; A. Bailey Hass ; G. Díaz Leines ; A. J. Archer

J. Chem. Phys. 158, 124114 (2023)
https://doi.org/10.1063/5.0135880

The Journal of Chemical Physics ARTICLE scitation.org/journal/jcp

Stochastic transitions: Paths over higher energy barriers can dominate in the early stages

Cite as: J. Chem. Phys. 158, 124114 (2023); doi: 10.1063/5.0135880
Submitted: 23 November 2022 • Accepted: 5 March 2023 •
Published Online: 28 March 2023

S. P. Fitzgerald,[1,a)] A. Bailey Hass,[1] G. Díaz Leines,[2] and A. J. Archer[3,b)]

AFFILIATIONS

[1] Department of Applied Mathematics, University of Leeds, Leeds LS2 9JT, United Kingdom
[2] Yusuf Hamied Department of Chemistry, University of Cambridge, Lensfield Road, Cambridge CB2 1EW, United Kingdom
[3] Department of Mathematical Sciences and Interdisciplinary Centre for Mathematical Modelling, Loughborough University, Loughborough, Leicestershire LE11 3TU, United Kingdom

[a)] **Author to whom correspondence should be addressed:** s.p.fitzgerald@leeds.ac.uk
[b)] a.j.archer@lboro.ac.uk

ABSTRACT

The time evolution of many physical, chemical, and biological systems can be modeled by stochastic transitions between the minima of the potential energy surface describing the system of interest. We show that in cases where there are two (or more) possible pathways that the system can take, the time available for the transition to occur is crucially important. The well-known results of the reaction rate theory for determining the rates of transitions apply in the long-time limit. However, at short times, the system can, instead, choose to pass over higher energy barriers with a much higher probability, as long as the distance to travel in phase space is shorter. We construct two simple models to illustrate this general phenomenon. We also apply a version of the geometric minimum action method algorithm of Vanden-Eijnden and Heymann [J. Chem. Phys. **128**, 061103 (2008)] to determine the most likely path at both short and long times.

I. INTRODUCTION

The transition dynamics of complex systems having many degrees of freedom can often be reduced to one or two reaction coordinates. These are the system degrees of freedom that evolve the slowest in time.[1] All the other (maybe very many) degrees of freedom are slaved to these slowest processes.[2] The slow evolution of these systems is usually characterized by rare transitions between metastable states separated by significant energy barriers. The identification of the reaction coordinates in high-dimensional (complex) systems remains extremely challenging.[3] For example, for large molecules, the center of mass is often a "slow" degree of freedom, while the fluctuations of the individual atoms within the molecule are the slaved "fast" degrees of freedom. This is the case, e.g., in biomolecular conformation changes, such as protein folding,[4,5] nucleation-driven phase transformations,[6] and surfactant molecules in a liquid transitioning from being freely dispersed in the liquid or joined together in a micelle or adsorbing to interfaces.[7–9] An example of recent work to identify the relevant reaction coordinates is Ref. 10, which uses machine learning. Of course, for high-dimensional systems, the energy landscape is often complex, with multiple critical points, barriers of various sizes, and multiple transition paths connecting the stable states. For such systems, algorithms based on simplifying assumptions, such as no barrier recrossings, single transition states, a smooth landscape, and "long enough" (infinite) times, often fail to provide a straightforward and accurate estimation of the rate[6] or to even identify the most likely path[11,12] under perturbations of the energy landscape.

We consider here a class of such stochastic dynamical systems where there is a simple choice of two transition pathways away from the initial state: one is over a smaller energy barrier (the activation energy barrier for chemical reactions), but the system has to evolve a greater distance in phase space (i.e., has a longer reaction pathway), while the other path is over a much higher energy barrier but has a much shorter distance to travel in phase space. The specific model systems of these types that we consider here are displayed in Figs. 1(a), 2(a), and 2(b). Examples of systems of this type include those where a surfactant molecule in a liquid has a choice between adsorbing to an interface or forming micelles or

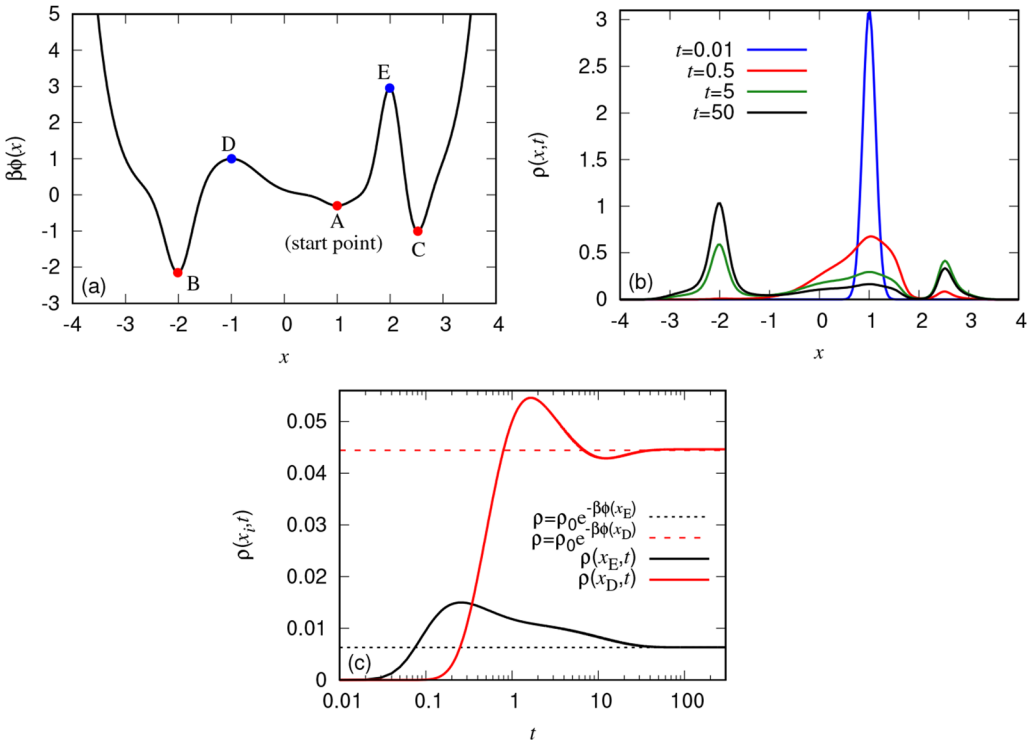

FIG. 1. (a) 1D model potential; (b) probability density $\rho(x,t)$ over time as the system evolves in the potential, having started at point A at time $t = 0$; (c) density at the two saddle points vs time with equilibrium $t \to \infty$ values also shown.

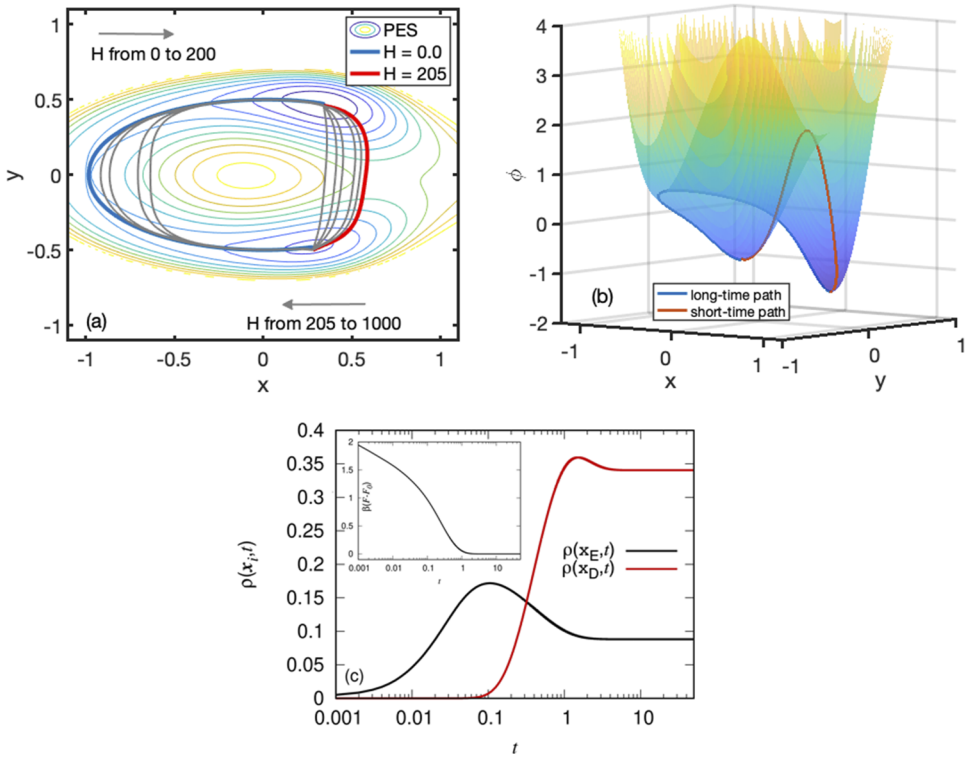

FIG. 2. (a) A contour plot of our 2D potential ϕ together with the modified gMAM results for the MLP, for various values of the path power H. (b) A surface plot of ϕ together with the $t \to \infty$ long-time MLP (over the lower barrier) and the short-time MLP for $H = 250$ (over the higher barrier). Note that the surface color scheme in (b) is the same as that used for the contours in (a). In (c), we plot the density at the two saddle points, $\rho(\mathbf{x}_D, t)$ and $\rho(\mathbf{x}_E, t)$, as a function of time t. The inset of (c) is a plot of the Helmholtz free energy difference $(F - F_0)$ over time, where $F_0 = F(t \to \infty)$.

those where a chemical reaction can proceed via a catalyzed or non-catalyzed route, e.g., where the presence of water surrounding the reacting molecules determines the reaction pathway and energy barrier height.[13] In the context of the Ginzburg–Landau equation and other related partial differential equation models for stochastic transitions, transition pathways conditioned on a specified timescale were considered in Ref. 14 and it was shown that, sometimes, the optimal paths contain large excursions.

The standard reaction-rate theory (RRT), which includes transition state theory and other related approaches,[2] predicts that the path over the lowest barrier is the most likely and, therefore, dominates the dynamics, at least for simple energy landscapes. However, even for these simple cases, we find that the standard RRT picture does not hold and the behavior crucially depends on the timescale over which the system is sampled. In particular, at shorter times (but still much longer than the timescale of the fluctuating "fast" degrees of freedom), the flux over the higher barrier can completely dominate the dynamics of the system and, even at intermediate times, the transition probabilities are very different from the predictions of RRT approaches, which do not consider the time taken; i.e., RRT only applies in the long-time limit. Due to this, even at timescales approaching those corresponding to lower-barrier crossings (as predicted by RRT), the contributions to the overall rate from crossings of the higher barrier can be significant, and so RRT does not give the whole picture. Thus, the key finding of our work is that the length of time over which barrier crossing problems are allowed to proceed is critically important. In any system where the reaction is stopped after a certain time, the reaction pathway predicted by RRT may not be the one actually taken. An example of this is the recent study of helium diffusion via hops between interstitial sites in PuO_2.[15] Here, the authors found that in a 1 ns time window, surprisingly 9 out of 12 of the transitions proceeded via a higher-energy pathway. Another situation where the time available may be critical is in the case of flow reactors such as catalytic converters. However, in any system that can explore the long-time limit, the predictions of RRT are fully recovered. Conversely, if the potential landscape and reaction coordinates are unknown and are inferred via densities and rates measured from experiments or simulations necessarily performed on a finite timescale, then the dominant long-time dynamics of the system may be missed entirely.

Additionally, we develop a method for calculating the most likely path (MLP) through the potential energy landscape, useful for analyzing systems with two or more dimensions. Various techniques to compute the minimum energy (and hence most probable) path between two minima exist, including the string method and the geometric minimum action method (gMAM;[16,17] see also Refs. 14, 18, and 19). Such paths, sometimes known as the *instanton*, are everywhere parallel to the potential gradient and correspond to the infinite-time transition. In this work, we extend the gMAM approach to finite-time transitions and derive a modified algorithm to compute finite-time, out-of-equilibrium paths. These are no longer parallel to the potential gradient and correspond to the most probable path conditioned on a finite duration. We find that these can be radically different from the instanton and may pass through completely different intermediate states. We explain how these paths are connected to the full transient dynamics of the system given by the Fokker–Planck equation.

II. THEORY FOR STOCHASTIC DYNAMICAL SYSTEMS

We demonstrate our findings with two simple generic toy models. The first is one-dimensional (1D), and the potential energy landscape has three minima. The system is initiated in the middle one and then has a choice to evolve either to the left or to the right. Our second model potential is two-dimensional (2D). It has two minima and two saddles, meaning two different classes of path linking one minimum to the other. One path is shorter but over a high barrier in the potential, while the other is further but over a much lower barrier. RRT would suggest that the second is the dominant transition pathway, but we find that this is not the case if one only considers the system for sufficiently short times. These systems are described by the overdamped stochastic equation of motion,

$$\Gamma^{-1}\frac{d\mathbf{x}}{dt} = -\nabla\phi(\mathbf{x}) + \boldsymbol{\eta}, \tag{1}$$

where $\mathbf{x}$ is the "slow" relevant degree of freedom of the system (1D or 2D in the cases considered here), $\phi(\mathbf{x})$ is the potential energy of the system (strictly speaking, in systems where the irrelevant "fast" degrees of freedom have been integrated out, ϕ is the constrained free energy), Γ^{-1} is a friction constant that, henceforth, we set equal to one (i.e., absorb it into the timescale), and $\boldsymbol{\eta}$ is a random force originating from thermal fluctuations in the system. This is modeled as a white noise with zero mean $\langle\eta_i(t)\rangle = 0$ and correlator $\langle\eta_i(t)\eta_j(t')\rangle = 2k_\mathrm{B}T\Gamma^{-1}\delta_{ij}\delta(t-t')$, where k_B is Boltzmann's constant and T is the temperature (i.e., the amplitude of the random fluctuations).

The Fokker–Plank equation for the probability density $\rho(\mathbf{x}, t)$ corresponding to Eq. (1) is[20]

$$\frac{\partial\rho}{\partial t} = \nabla\cdot[k_\mathrm{B}T\nabla\rho + \rho\nabla\phi]. \tag{2}$$

When $\phi = 0$, this becomes $\frac{\partial\rho}{\partial t} = D\nabla^2\rho$, the diffusion equation, with diffusion coefficient $D = \Gamma k_\mathrm{B}T$. Note that Eq. (2) can be written as a gradient flow,

$$\frac{\partial\rho}{\partial t} = \nabla\cdot\left[\rho\nabla\frac{\delta F}{\delta\rho}\right], \tag{3}$$

with the Helmholtz free energy functional

$$F[\rho] = \int \rho[k_\mathrm{B}T\,\ln\rho + \phi]\mathrm{d}^n\mathbf{x}, \tag{4}$$

which is a Lyapunov functional for the dynamics in n dimensions. Note that these are the equations of dynamical density functional theory.[21–23] For a given potential $\phi(\mathbf{x})$, the equilibrium density is $\rho(\mathbf{x}) = \rho_0 e^{-\beta\phi(\mathbf{x})}$, where $\beta = (k_\mathrm{B}T)^{-1}$ and ρ_0 is a constant determined by the normalization of $\rho(\mathbf{x})$; i.e., $\rho_0^{-1} = \int e^{-\beta\phi(\mathbf{x})}\mathrm{d}^n\mathbf{x}$.

When $\phi(\mathbf{x})$ has at least two minima, the quantity of interest is the typical waiting time to observe transitions between the minima. The standard RRT states that this transition rate k is given by the Arrhenius (or Kramers) relation $k = \nu\exp(-\beta\Delta\phi)$, where $\Delta\phi \equiv \phi(\mathbf{x}_s) - \phi(\mathbf{x}_A)$ is the height of the barrier, with $\mathbf{x}_A$ being the

position of the minimum and $\mathbf{x}_s$ being the maximum (more generally, the saddle-point) on the barrier. The prefactor ν depends on various factors,[2] but it is the exponential that crucially determines the rate and can be thought of as originating from the ratio $\rho(\mathbf{x}_s)/\rho(\mathbf{x}_A)$, which is the probability of finding the system on the barrier divided by the probability of it being at the minimum. However, this ratio $\propto \exp(-\beta\Delta\phi)$ only in the long time $t \to \infty$ limit. Solving Eq. (2) with the initial condition $\rho(\mathbf{x}, t = 0) = \delta(\mathbf{x} - \mathbf{x}_A)$, we find that the RRT result can be completely wrong in some cases if considering transitions with only a short time to occur.

III. RESULTS FOR 1D MODEL

We first consider the 1D potential $\phi(x)$ in Fig. 1(a); the equation for $\phi(x)$ is given in the Appendix. This potential has three minima [labeled A, B, and C in Fig. 1(a)] at $x_B \approx -2$, $x_A \approx 1$, and $x_C \approx 2.5$ and two maxima (labeled D and E) at $x_D \approx -1$ and $x_E \approx 2$. We initiate the system in the minimum at A. It can then either move to the right, over the much higher energy barrier at E, or it can go to the left over the lower barrier at D. Going left, it has further to travel.

In Fig. 1(b), we plot the density profile $\rho(x, t)$ obtained from solving Eq. (2) (using a simple finite difference scheme) for a sequence of different times t. Rather than initiating the system with the Dirac δ-distribution centered at x_A, we use a narrow Gaussian corresponding to a free diffusion for the short initial time $t = 0.01$. By the time $t = 0.5$, we see a sizable peak in $\rho(x, t)$ at C, the right-hand minimum in $\phi(x)$, but very little density has made it to the minimum at B. This is because B is further away, so in the early stages, the system is more likely to cross the barrier at E, despite it being higher than the barrier at D. It takes until $t \approx 30$ for $\rho(x, t)$ to cease evolving in time and the system to reach the equilibrium distribution. Note also that, at $t = 5$, the density at C is *higher* than its eventual equilibrium value. Once the system has "found" the lower-energy minimum at B, the density moves back over the high barrier at E to approach $\rho_0 e^{-\beta\phi(\mathbf{x})}$.

In Fig. 1(c), we plot the densities at the points D and E over time. These are the locations of the two potential maxima (the barriers). We see that at early times $t \sim 0.1$, the probability of being at the highest maximum E is sizable and well above the RRT probability $\sim \exp[-\beta\phi(x_E)]$, while the probability of being at the lower maximum D is still ≈ 0, in contrast to the RRT prediction that the probability $\sim \exp[-\beta\phi(x_D)]$. Even at $t \sim 1$, the RRT predictions are still incorrect.

IV. RESULTS FOR 2D MODEL

We also consider a system evolving in the 2D potential displayed in Fig. 2; the precise expression for this potential is given in the Appendix. Figure 2(a) shows a contour plot, while Fig. 2(b) is a surface plot. This potential has a local minimum at point A, $(x_A, y_A) = (0.38, -0.47)$, and the global minimum at B, $(x_B, y_B) = (0.42, 0.47)$. There is a local maximum near the origin. We initiate the system at A. There are two routes to go from A to B: the long route, round to the left in Fig. 2(a), through the saddle at point D, $(x_D, y_D) = (-1, 0)$, or the short route to the right through the saddle at point E at $(x_E, y_E) = (0.67, 0)$. The barrier height to the left

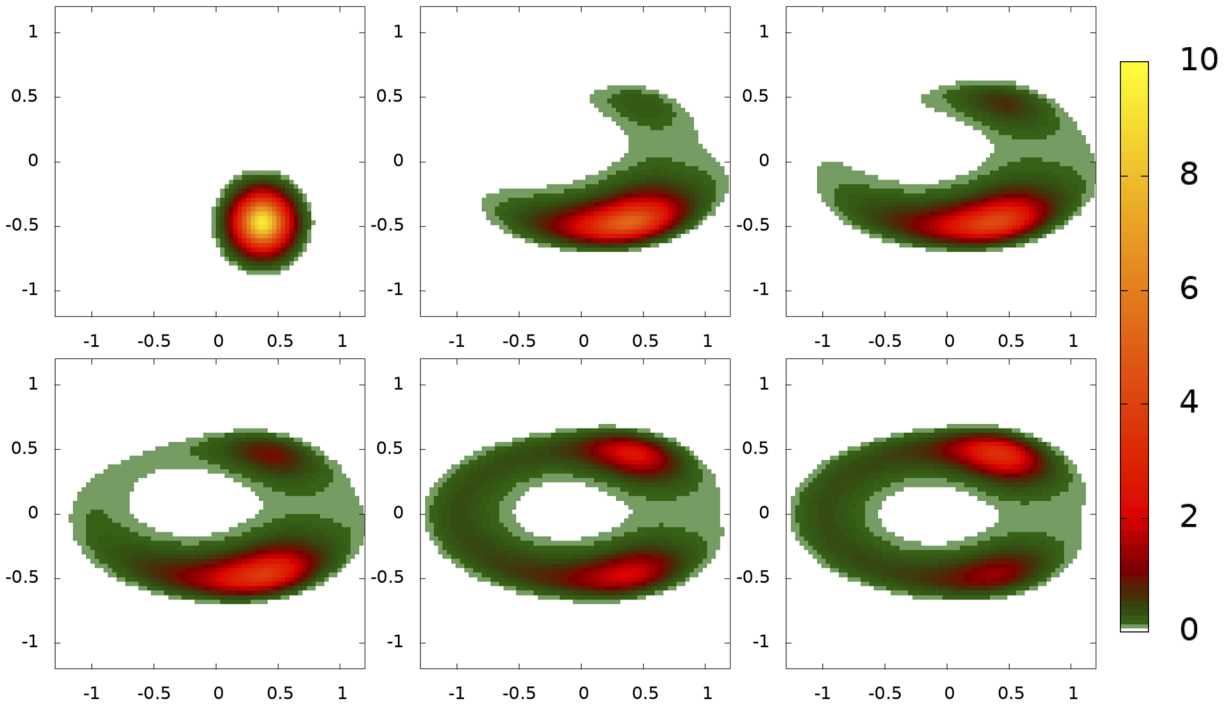

FIG. 3. Density profile $\rho(x, y, t)$ at the times $t = 0.01$, 0.02, 0.03, 0.04, 0.1, and 5, going from top left to bottom right, for our 2D potential.

is much lower, with $\beta\Delta\phi = 1.4$. In contrast, the barrier to the right is twice as high, with $\beta\Delta\phi = 2.8$. Nonetheless, we see from Fig. 2(c), which shows the density at the two saddle points (i.e., the tops of the two transition barriers) over time, that at early times, the system is more likely to take the shorter route to the right, even though it is over the higher barrier. Note how similar Fig. 2(c) is to Fig. 1(c). In the inset of Fig. 2(c), we plot the free energy [Eq. (4)] over time, which, as expected, decreases monotonically over time. In Fig. 3, we display the density profiles over time. These again show that at early times, the probability for the particle to be at the higher barrier at point E is much greater than at the lower barrier at D.

Just as Fig. 1 shows for the 1D model, Fig. 3 shows for the 2D model that at later times, there are contributions to the dynamics from returning over the two barriers to the start point. One can calculate the total flux crossing any line on the 2D surface since from Eq. (3), we can obtain the flux as $\mathbf{j} = -\rho\nabla\frac{\delta F}{\delta\rho}$. However, because we can only calculate the net flux and not the individual fluxes going forward and backward over the barriers, the plots of the total flux for our 2D model do not give us much additional insight and so are not displayed.

V. PATH INTEGRAL FORMULATION

Stochastic processes can also be investigated using an action formalism,[24,25] in analogy with the path integral formulation of quantum mechanics.[26] The MLP can be determined by minimizing an action over the space of paths, as described by the minimum action method (MAM) in Ref. 14. That work developed a general large deviation theory for fields (e.g., the Ginzburg–Landau model and the Brusselator), valid in the limit of small noise. The original MAM method computes transition paths for any finite time, but the infinite-time (i.e., RRT) limit is difficult to handle. The geometric reformulation (gMAM[16,17]) addresses this. To further elucidate our findings from Secs. III and IV, i.e., that the finite-time transitions can proceed via different paths from those suggested by the long-time limit of RRT, we now modify the gMAM algorithm to include finite transition times while retaining the geometric formulation. An appealing feature of this for finite-time paths is that it allows a correspondence between the MLPs in the stochastic system and the solutions of Hamilton's equations in an effective potential to be straightforwardly exploited. We introduce this formalism below.

The Gaussian white noise $\boldsymbol{\eta}$ in Eq. (1) has a probability density functional $\mathcal{P}[\boldsymbol{\eta}] \sim \exp\left[-\frac{1}{4k_BT}\int_0^t \boldsymbol{\eta}\cdot\boldsymbol{\eta}\,\mathrm{d}\tau\right]$. Substituting (1) into this, we immediately obtain

$$\mathcal{P}[\mathbf{x}] \sim \exp\left[-\frac{1}{4k_BT}\int_0^t |\dot{\mathbf{x}} + \nabla\phi|^2\,\mathrm{d}\tau\right] \equiv \exp\left[-\frac{\mathcal{S}[\mathbf{x}]}{4k_BT}\right], \tag{5}$$

for the probability weight attached to a path $\mathbf{x}(\tau)$, and we have defined the *path action* $\mathcal{S}$. The transition probability $P(\mathbf{x}_1, t|\mathbf{x}_0, 0)$ can now be written as a path integral,[24,25]

$$P(\mathbf{x}_1, t|\mathbf{x}_0, 0) = \int \mathcal{D}\mathbf{x}\,\mathcal{J}[\mathbf{x}]\,\exp\left[-\frac{\mathcal{S}[\mathbf{x}]}{4k_BT}\right] \tag{6}$$

where $\mathcal{J} = |\delta\boldsymbol{\eta}/\delta\mathbf{x}|$ is the functional Jacobian arising from the change of variables $\boldsymbol{\eta} \to \mathbf{x}$ and the integral $\mathcal{D}\mathbf{x}$ is taken over all paths $\mathbf{x}(\tau)$ with endpoints $\mathbf{x}(0) = \mathbf{x}_0$ and $\mathbf{x}(t) = \mathbf{x}_1$. Note that some constants are absorbed into the functional measure. This expression solves the Fokker–Planck Eq. (2) with the initial condition $\rho(\mathbf{x}, 0) = \delta(\mathbf{x} - \mathbf{x}_0)$ but cannot be evaluated exactly except for simple special cases, such as quadratic ϕ. However, we are primarily interested in transitions that require a significant energy barrier to be surmounted, where the action is, hence, typically much larger than k_BT, and so the integral is dominated by paths that minimize $\mathcal{S}$, i.e., paths that satisfy the Euler–Lagrange equations for $\mathcal{S}$,

$$\ddot{\mathbf{x}} = \nabla\phi\,\nabla\nabla\phi; \qquad |\dot{\mathbf{x}}|^2 - |\nabla\phi|^2 = H, \tag{7}$$

where $\nabla\nabla\phi$ is the Hessian matrix of ϕ. These correspond to the (conservative) Hamiltonian motion of a particle of mass 2 (actually, 2× friction[2]) moving in an effective potential $F = -|\nabla\phi|^2$, and the quantity H is conserved along the path.[27] H is analogous to the energy in the effective system but has the dimensions of a power. Note that here we are really saying that the dominant (non-differentiable) paths lie within a small tube around the solution to (7)[28] and the fluctuations around this can be integrated over to determine the pre-exponential (entropic) factor in the transition rate—see, e.g., Ref. 26. Here, we focus on determining the MLPs, rather than the rates themselves, and extend the gMAM algorithm to incorporate the constraint of finite time. This stochastic–Hamiltonian correspondence has also been explored in Ref. 29, where an alternative path-finding algorithm was developed. This approach expresses the space of paths using Chebyshev polynomials and minimizes the action using a Ritz method. Inserting Eq. (7) into the action integral yields

$$S = 2[\phi(\mathbf{x}_1) - \phi(\mathbf{x}_0)] - Ht + 2\int_\gamma \sqrt{H + |\nabla\phi|^2}\,|\mathrm{d}\mathbf{x}|, \tag{8}$$

with the time for the path given by

$$t = \int_\gamma \frac{|\mathrm{d}\mathbf{x}|}{\sqrt{H + |\nabla\phi|^2}}. \tag{9}$$

S is Hamilton's principal function for effective classical mechanics and corresponds to the large deviation rate function for stochastic dynamics. γ is the optimal path through the potential linking $\mathbf{x}_0$ and $\mathbf{x}_1$, i.e., the solution of (7). The relation between the path power H and the time t comes from either solving the classical equation of motion or extremizing S over H. $t \to \infty$ corresponds to $H \to 0$, provided that the path includes a critical point of ϕ, which is the case for the transitions of interest. When $H = 0$, $\dot{\mathbf{x}} = \pm\nabla\phi$, and γ is the minimum energy path, which can be determined using, e.g., gMAM.[16] This path corresponds to $t \to \infty$ and the long-time average rate, since

$$S \to 2\Delta\phi + 2\int_\gamma |\nabla\phi|\,|\mathrm{d}\mathbf{x}| = \begin{cases} 0, & \text{downhill path,} \\ 4\Delta\phi > 0, & \text{uphill path,} \end{cases} \tag{10}$$

where $\Delta\phi = \phi(\mathbf{x}_1) - \phi(\mathbf{x}_0)$. The last equality follows from the fact that, for $H = 0$, the path is always (anti-)parallel to $\nabla\phi$ (note that the converse to this statement is not necessarily true). This zero-power path, the instanton, recovers the familiar Kramers form $\exp(-\beta\Delta\phi)$ for the average rate at which an energy barrier of height $\Delta\phi$ is traversed. Different values of H correspond to different paths; the

equation of motion $\ddot{\mathbf{x}} = -\nabla F$ has different boundary conditions. We now refer to the path as γ_H, and note that γ_0 is the absolute minimum action path determined by the original gMAM algorithm. In particular, the initial and final velocity vectors for γ_H have different magnitudes and directions from those of γ_0, which start and end at rest.

The gMAM algorithm[11,16,17] can be modified to include paths with nonzero power H as follows: following the notation of Ref. 16, parameterize the curve γ_H by a normalized arc length using $\alpha \in [0,1]$, and let $\mathbf{X}(\alpha) = (X_1(\alpha), X_2(\alpha), \ldots)$ be the parametric equations of the curve. The path-dependent part of the action can be written as

$$\begin{aligned} S - 2\Delta\phi &= -Ht + 2\int_\gamma \sqrt{H + |\nabla\phi|^2}\,|\mathrm{d}\mathbf{X}| \\ &= \int_\gamma \frac{H + 2|\nabla\phi|^2}{\sqrt{H + |\nabla\phi|^2}}\,|\mathrm{d}\mathbf{X}| \\ &= \int_0^1 g(\alpha)\,\mathbf{X}'^2(\alpha)\;\mathrm{d}\alpha, \end{aligned} \tag{11}$$

where the prime denotes differentiation with respect to α and

$$g(\alpha) = \frac{1}{|\mathbf{X}'(\alpha)|}\,\frac{H + 2|\nabla\phi|^2}{\sqrt{H + |\nabla\phi|^2}}. \tag{12}$$

The Euler–Lagrange equation for $\mathbf{X}(\alpha)$ then reads

$$\frac{\delta S}{\delta X_i} = \frac{1}{g}(\nabla\phi)_j(\nabla\nabla\phi)_{ji}\frac{(H + 2|\nabla\phi|^2)(3H + |\nabla\phi|^2)}{(H + |\nabla\phi|^2)^2} - \left(gX_i'\right)' = 0, \tag{13}$$

and $\mathbf{X}$ is evolved from an initial guess (e.g., the straight line from $\mathbf{x}_0$ to $\mathbf{x}_1$, although other initial configurations can be used) according to

$$\frac{\mathrm{d}\mathbf{X}}{\mathrm{d}\tau} = -g\frac{\delta S}{\delta \mathbf{X}}. \tag{14}$$

The factor of $g > 0$ avoids potential numerical issues when H and $\nabla\phi$ become small. Full details can be found in Ref. 16, where the authors also present a robust and efficient numerical implementation that avoids the computation of the Hessian $\nabla\nabla\phi$. Note that Ref. 11 investigates the convergence of gMAM as compared with the string method, finding that gMAM more reliably identifies the MEP in complex landscapes, independently of the initial guess.

Because H is defined implicitly in Eq. (9) and the path γ_H depends on H, it cannot be determined *a priori*. If the time t is specified, a further iterative process would be required to find H. For simple 1D paths, t is a decreasing function of H and a simple bisection would suffice, but in higher dimensions, it is not as simple since different values of H can produce very different paths. As H becomes large, it is much greater than all values of $|\nabla\phi|^2$ and so the path γ_H becomes the straight line from $\mathbf{x}_0$ to $\mathbf{x}_1$.

In Figs. 2(a) and 2(b), we display the MLP for various H, i.e., for various values of t, obtained from our extended gMAM algorithm (a simple implementation in `matlab` takes a few minutes on a laptop for these simple 2D examples; higher-dimensional calculations would require a more sophisticated implementation). The blue $H = 0$ path corresponds to $t \to \infty$, which is the MLP predicted by RRT. As H is increased, we see from Fig. 2(a) that the MLP no longer passes through the saddle point (the transition state of RRT) at $\mathbf{x}_D = (-1, 0)$, instead cutting the corner. For $H \geq 205$, we see that the MLP jumps to the other side of the potential and no longer goes anywhere near point D and, instead, goes in the vicinity of point E, i.e., over the much higher energy barrier; see, e.g., the $H = 205$ red path in Fig. 2(a), which has the corresponding time $t = 0.047$. The same paths are obtained whether starting from either a straight line or an initial path chosen to be close to the infinite-time RRT path. For times of order $t \sim 0.1$, we find that paths via either route have roughly the same path action, despite having very different barrier heights. The convergence time was not significantly affected in this case, though could be in others. An adaptive "time" step could be added to accelerate the algorithm in cases with flat regions of S in path space. Importantly, the action for the paths on either side of the $H \in [200, 205]$ bifurcation is very similar, although the path times differ significantly. This implies a fairly large time window from $t \approx 0.05$ to $t \approx 0.17$, where a similar amount of flux crosses both barriers. For $t < 0.05$, the higher saddle dominates, and for $t > 0.17$, the lower saddle dominates. The order of magnitude of this time is in agreement with what we see in Fig. 2(c), from solving Eq. (2), i.e., the time when the densities at the two saddle points are equal. In the Appendix, we give the values of H used together with the corresponding times t. This is all consistent with Fig. 3, which shows the density ρ calculated by solving Eq. (2) directly for a range of times t (again using a finite difference scheme). Note that these calculations determine the entire density, assuming that this can be written in the WKB form $\rho = A\exp(-S/k_\mathrm{B}T)$, where the prefactor A depends, in some non-exponential way, on T. As $k_\mathrm{B}T \to 0$, the exponential term dominates the transition probability, but at finite $k_\mathrm{B}T$, one should not expect exact quantitative agreement between the two approaches since the path-finding algorithm only determines the action S. It ought to be possible to compute fluctuations around the dominant path[25,26] to determine A as $k_\mathrm{B}T \to 0$, although this is beyond the scope of this article. Moreover, the path-finding methods, such as the modified gMAM presented here and in Ref. 29, can be applied, in principle, to arbitrarily high dimensions, whereas the direct integration of the Fokker–Planck equation quickly becomes computationally intractable.

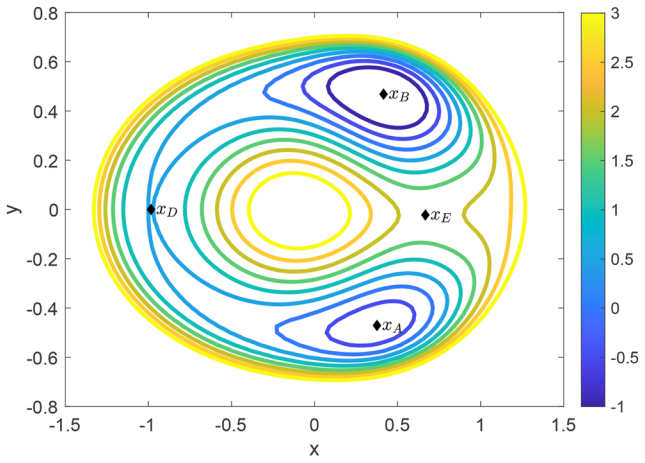

FIG. 4. 2D model potential; see Eq. (A2)

VI. CONCLUDING REMARKS

We have shown that the important difference between the finite-time minimum action paths and their infinite-time limit, the instanton, is that conditioned on a finite time, the minimum action (and hence most probable) path need not traverse the lowest energy barrier. Although the instanton is the path from $\mathbf{x}_0$ to $\mathbf{x}_1$ involving the absolute minimum of hill-climbing, when constrained to a finite time, a shorter path may be worth the extra uphill. This has implications for any stochastic transition where only a finite time is available for the reaction to occur, particularly if there are several paths the system can take. Moreover, transition paths and energy barriers inferred from experiments or simulations conducted over too short a timescale could easily be very different from the paths and barriers that dominate the system dynamics in reality.

ACKNOWLEDGMENTS

S.P.F. acknowledges the support from the UK EPSRC, Grant No. EP/R005974/1. We benefited from valuable discussions with Tapio Ala-Nissila, Thomas Bartsch, Rob Jack, Celia Reina, Roger Smith, and Uwe Thiele.

AUTHOR DECLARATIONS

Conflict of Interest

The authors have no conflicts to disclose.

Author Contributions

S. P. Fitzgerald: Conceptualization (equal); Funding acquisition (equal); Investigation (equal); Methodology (equal); Project administration (equal); Software (equal); Supervision (equal); Validation (equal); Visualization (equal); Writing – original draft (equal); Writing – review & editing (equal). **A. Bailey Hass**: Formal analysis (equal); Investigation (equal); Software (equal); Visualization (equal). **G. Díaz Leines**: Formal analysis (equal); Software (equal); Visualization (equal); Writing – review & editing (equal). **A. J. Archer**: Conceptualization (equal); Formal analysis (equal); Investigation (equal); Methodology (equal); Resources (equal); Software (equal); Visualization (equal); Writing – original draft (equal); Writing – review & editing (equal).

DATA AVAILABILITY

The data that support the findings of this study are available from the corresponding author upon reasonable request.

APPENDIX: MODEL POTENTIALS

In this appendix, we give further details about the model potentials studied and also a table of times t corresponding to path powers H.

1. 1D model potential

The 1D potential that we consider, displayed in Fig. 1, is

$$\beta\phi(x) = \left(\frac{x}{3}\right)^{10} + e^{-2(x+1)^2} + 3e^{-12(x-2)^2} - \frac{13}{10}e^{-12(x-2.5)^2} - \frac{3}{10}e^{-8(x-1)^2} - \frac{23}{10}e^{-8(x+2)^2}. \tag{A1}$$

The precise locations of the three minima are $x = x_B = -2.011\,726\,4$ (the global minimum), $x = x_A = 1.000\,428\,8$ (a local minimum and our start point), and $x = x_C = 2.522\,979\,7$ (a local minimum), and the two local maxima are at $x = x_D = -0.997\,087\,09$ and $x = x_E = 1.991\,297\,8$.

The potential above was chosen so that there is roughly an order of magnitude separation in the times it takes to reach each of the two target minima. If they are any closer, the timescale separation is not so clear. On the other hand, an even greater timescale separation can be achieved by moving the left-hand minimum even further to the left. A similar procedure was followed in constructing the 2D potential below.

2. 2D model potential

The 2D potential that we consider, displayed in Figs. 2 and 4, is

$$\beta\phi(x,y) = 4(x^2+4y^2-1)^2 - \frac{1}{2}x - 2e^{-4\left(x-\frac{1}{2}\right)^2-4\left(y-\frac{1}{2}\right)^2} - e^{-4\left(x-\frac{1}{2}\right)^2-4\left(y+\frac{1}{2}\right)^2} + 3e^{-4(x-1)^2-4y^2}. \tag{A2}$$

This potential has two minima at $\mathbf{x}_A = (x_A, y_A) = (0.376\,106\,59, -0.470\,945\,57)$ (a local minimum and our start point) and $\mathbf{x}_B = (x_B, y_B) = (0.415\,640\,13, 0.468\,367\,80)$ (the global minimum).

The 2D potential has a local maximum near the origin at $\mathbf{x} = (-0.097\,396\,665, -0.005\,372\,7757)$, and there are two saddle points at $\mathbf{x}_D = (x_D, y_D) = (-0.983\,928\,63, -0.000\,107\,741\,53)$ and $\mathbf{x}_E = (x_E, y_E) = (0.667\,212\,35, -0.022\,398\,035)$.

In Table I, we give the times t corresponding to various values of the path power H. Some of these paths are also displayed in Fig. 2(a).

TABLE I. Time t for various H values.

H	0	0.01	0.02	0.03	0.1	2.5	5.0	10.0	25.0	50.0	100.0
t	∞	7.84	6.85	6.28	4.70	1.61	1.21	0.888	0.575	0.405	0.277
H	195.0	200.0	205.0	212.0	235.0	245.0	250.0	300.0	400.0	500.0	1000.0
t	0.153	0.165	0.0478	0.0463	0.0419	0.0402	0.0413	0.0338	0.0255	0.0221	0.0168

REFERENCES

[1] B. Peters, *Reaction Rate Theory and Rare Events* (Elsevier, 2017).
[2] P. Hänggi, P. Talkner, and M. Borkovec, "Reaction-rate theory: Fifty years after Kramers," Rev. Mod. Phys. **62**(2), 251 (1990).
[3] J. Rogal, "Reaction coordinates in complex systems-a perspective," Eur. Phys. J. B **94**(11), 223 (2021).
[4] S. S. Cho, Y. Levy, and P. G. Wolynes, "P versus Q: Structural reaction coordinates capture protein folding on smooth landscapes," Proc. Natl. Acad. Sci. U. S. A. **103**(3), 586–591 (2006).
[5] K. A. Dill and J. L. MacCallum, "The protein-folding problem, 50 years on," Science **338**(6110), 1042–1046 (2012).
[6] K. E. Blow, D. Quigley, and G. C. Sosso, "The seven deadly sins: When computing crystal nucleation rates, the devil is in the details," J. Chem. Phys. **155**(4), 040901 (2021).
[7] J. N. Israelachvili, *Intermolecular and Surface Forces* (Academic Press, 2011).
[8] L. G. Leal, *Advanced Transport Phenomena: Fluid Mechanics and Convective Transport Processes* (Cambridge University Press, 2007), Vol. 7.
[9] U. Thiele, A. J. Archer, and L. M. Pismen, "Gradient dynamics models for liquid films with soluble surfactant," Phys. Rev. Fluids **1**, 083903 (2016).
[10] J. H. Appeldorn, S. Lemcke, T. Speck, and A. Nikoubashman, "Employing artificial neural networks to identify reaction coordinates and pathways for self-assembly," J. Phys. Chem. B **126**, 5007–5016 (2022).
[11] G. Díaz Leines and J. Rogal, "Comparison of minimum-action and steepest-descent paths in gradient systems," Phys. Rev. E **93**(2), 022307 (2016).
[12] X. Liu, H. Chen, and C. Ortner, "Stability of the minimum energy path," arXiv:2204.00984 (2022).
[13] G. Li, B. Wang, and D. E. Resasco, "Water-mediated heterogeneously catalyzed reactions," ACS Catal. **10**(2), 1294–1309 (2019).
[14] W. E, W. Ren, and E. Vanden-Eijnden, "Minimum action method for the study of rare events," Commun. Pure Appl. Math. **57**(5), 637–656 (2004).
[15] E. Murray, Y. Zhou, P. Slater, R. Smith, P. Goddard, and H. Steele, "Atomistic simulation of helium diffusion and clustering in plutonium dioxide," Phys. Chem. Chem. Phys. **24**(35), 20709–20720 (2022).
[16] E. Vanden-Eijnden and M. Heymann, "The geometric minimum action method for computing minimum energy paths," J. Chem. Phys. **128**(6), 061103 (2008).
[17] M. Heymann and E. Vanden-Eijnden, "The geometric minimum action method: A least action principle on the space of curves," Commun. Pure Appl. Math. **61**(8), 1052–1117 (2008).
[18] P. Koehl, "Minimum action transition paths connecting minima on an energy surface," J. Chem. Phys. **145**(18), 184111 (2016).
[19] R. Olender and R. Elber, "Yet another look at the steepest descent path," J. Mol. Struct.: THEOCHEM **398**, 63–71 (1997).
[20] C. W. Gardiner, *Handbook of Stochastic Methods* (Springer Berlin, 1985), Vol. 3.
[21] M. te Vrugt, H. Löwen, and R. Wittkowski, "Classical dynamical density functional theory: From fundamentals to applications," Adv. Phys. **69**(2), 121–247 (2020).
[22] A. J. Archer and R. Evans, "Dynamical density functional theory and its application to spinodal decomposition," J. Chem. Phys. **121**(9), 4246–4254 (2004).
[23] U. M. B. Marconi and P. Tarazona, "Dynamic density functional theory of fluids," J. Chem. Phys. **110**(16), 8032–8044 (1999).
[24] H. S. Wio, *Path Integrals for Stochastic Processes: An Introduction* (World Scientific, 2013).
[25] R. Graham, "Path integral formulation of general diffusion processes," Z. Phys. B Condens. Matter **26**(3), 281–290 (1977).
[26] L. S. Schulman, *Techniques and Applications of Path Integration* (Courier Corporation, 2012).
[27] H. Ge and H. Qian, "Analytical mechanics in stochastic dynamics: Most probable path, large-deviation rate function and Hamilton–Jacobi equation," Int. J. Mod. Phys. B **26**(24), 1230012 (2012).
[28] R. L. Stratonovich, "On the probability functional of diffusion processes," Sel. Trans. Math. Stat. Prob. **10**, 273–286 (1971).
[29] L. Kikuchi, R. Singh, M. E. Cates, and R. Adhikari, "Ritz method for transition paths and quasipotentials of rare diffusive events," Phys. Rev. Res. **2**(3), 033208 (2020).